Vacuum 225 (2024) 113274

Contents lists available at ScienceDirect

Vacuum

journal homepage: www.elsevier.com/locate/vacuum

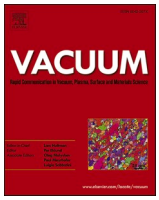

Cylindrical hot cathode ionisation gauge – Construction and testing

Ricardo A.S. Silva [a,*], Nenad Bundaleski [a], Berthold Jenninger [b], Orlando M.N.D. Teodoro [a]

[a] CeFiTec, Department of Physics, Nova School of Science & Technology, Nova University Lisbon, 2829-515, Caparica, Portugal
[b] CERN European Organization for Nuclear Research, 1211, Geneva, 23, Switzerland

ARTICLE INFO

Handling Editor: Oleg Malyshev

Keywords:
Ionisation gauge
Vacuum measurement
Accuracy
Stability
Metrological performance
Secondary electron suppression

ABSTRACT

Hot cathode ionisation gauges are indispensable in measuring high and ultra-high vacuum. In the present work the construction details and the metrological evaluation of a novel gauge design — the cylindrical ionisation gauge is presented. With the aim of enhancing accuracy and stability both in the short and long term, details of the mechanical assembling of electrodes and precautions to minimize leakage currents influencing ion current measurement are described. Performance evaluations demonstrate high short-term stability, with linearity error, reproducibility, and repeatability values consistently below 1 %, placing the gauge at the same level as the most stable ionisation gauges. Operating across a pressure range of at least 6 orders of magnitude, the gauge exhibits low linearity error from high to ultra-high vacuum ranges. Its capability to measure pressures below 10^{-9} mbar remains open and requires further investigation.

1. Introduction

Hot cathode ionisation vacuum gauges are commonly used as pressure measurement devices in high vacuum, becoming essential in the ultra-high vacuum range [1,2]. The general idea of measuring the concentration of particles in a chamber from the ion current created by electron impact is about 100 years old [3]. These devices have been developed in parallel with other vacuum technologies, to fulfil the ever-growing demands of the science and industry regarding accuracy, stability, measuring range, and operation under harsh conditions (e.g. in the presence of high magnetic fields [4]).

The reduction of the low pressure limit motivated the massive replacement of triode gauges [3] by Bayard-Alpert gauges [5] and, later on, by the extractor [6]. Further developments as the Helmer [7], ion spectroscopy [8] (including its simplified commercial version [9]) and AxTRAN [10] had the same motivation. Another example is the increased stability and accuracy offered by the Stabil-Ion gauge [11], which is constructed on the basis of the Bayard-Alpert configuration. The later is characterised by a highly robust design resisting to geometry changes during long-term operation, being consistent with the fact that one of the key factors determining the stability of ionisation gauges is the stability of the mean electron path length [12].

Electron trajectories in Bayard-Alpert and extractors gauges display a large distribution on their path length. As shown by simulations, although some electrons have short pathlengths, others pass the grid several times before an ionisation event or hitting the grid wire. Changes in the grid geometry or in the filament modifies the electron path and, therefore, the gauge reading, decreasing its accuracy. A further solution for the demand in accuracy is securing that all electrons have a single pass in the useful ionisation volume following a parallel trajectory. This strategy was implemented for the first time by Klopfer [13] and used in the recently proposed "ISO" gauge [14–16]. It has a clear advantage of more efficient protection of the ion collector from the influence of secondary particles (X-ray photons, electrons and ions) thus providing a potential benefit in reducing the low pressure limit. Numerous tests performed in the meantime confirm its overall uncertainty within 1 % for various gases [15].

The same concept was further explored by the authors when the design of a cylindrical hot cathode ionisation gauge was introduced [17]. The proposed design aims to enhance the measurement accuracy and reduce the short-term and long-term sensitivity drifts, thereby minimizing the need for frequent calibration, when compared to common gauges. These goals are pursued through the reduction, or even suppression, of the major unwanted effects of the physical phenomena inherent to any ionisation gauge. High performance and long-term stability are also strongly correlated with construction details, including materials selection, mechanical robustness, and high electrical insulation. The present work describes the relevant construction details as well as the metrological evaluation of this new gauge.

* Corresponding author.
E-mail address: ras.silva@campus.fct.unl.pt (R.A.S. Silva).

https://doi.org/10.1016/j.vacuum.2024.113274
Received 1 February 2024; Received in revised form 7 May 2024; Accepted 8 May 2024
Available online 11 May 2024

2. Geometrical configuration

Fig. 1 represents the working principle, including the electrode voltages optimised under simulation. Briefly, the proposed design is based on a belt-like beam of electrons emitted by a linear filament, following a circular path between two cylindrical electrodes, similarly to a cylindrical electrostatic energy analyser. Ions created by electron impact are accelerated by the radial electric field crossing the outer electrode, made of a mesh, reaching the ion collector. An additional mesh is added before the ion collector to suppress the secondary electrons. The measured ion current is therefore directly proportional to the particle concentration in the ionisation gauge, that is, to pressure. The key features of this configuration are.

1. Well-defined electron trajectories with a stable pathlength;
2. Lack of direct line of sight between the ion collector, the electron emitter and the Faraday cup, which reduces the low pressure limit imposed by X-rays or secondary charged particles;
3. It suppresses the ion induced secondary electrons providing high accuracy without the need of conditioning;
4. A linear filament as cathode, which, given the gauge's geometry, prevents changes in the electron path length induced by an eventual drift of the emission area.

The mechanical design took into consideration the following details: (1) it should prevent misalignments between electrodes, whilst being resistant to deformations; (2) good electrical insulation of electrodes, particularly of the ion collector; (3) sufficient conductance so the pressure difference between ionisation volume and vacuum chamber is negligible. The construction details addressing these points are discussed in the following subsections.

2.1. Mechanical assembling and electrical insulation

Details of the mechanical construction are presented in Fig. 2. The gauge is shielded inside a cylindrical envelope providing mechanical support for all electrodes. The envelope is also essential for the general stability of the gauge, shielding its interior from external electric fields that could impact its operation and preventing leaks of charged particles to the vacuum chamber [18]. Electrodes were made of 316L stainless steel having a section of a cylindrical surface and a planar base. All electrodes are fixed by its base to the envelope and spaced apart by ceramic balls, 5 mm in diameter. Each gap has 3 balls above and below each electrode inserted in 4 mm holes displaced at 120° from each other, as can be seen in Fig. 2b. This results in a 3 mm gap between electrodes. The whole sandwich is fastened to the bottom of the envelope using 3 assembling bolts.

As the emitter box and the deflector are not concentric cylinders with the gauge and can have the same voltage a ring was used to mechanically support them (Fig. 2c). This ring is the upper electrode of the sandwich structure presented in Fig. 2b which is compressed by the 3 bolts. The bolt heads are insulated from the top ring by ceramic bushings. The ring features perforations where the electrodes are fastened at precise positions, ensuring reliable alignment and securing proper functioning of the device. The emitter box, in turn, supports an 11 mm long linear filament as cathode, insulated from it. For the filament, a 0.15 mm diameter thoriated tungsten wire was used. A backplate was spot welded to one of the filament pins to properly define the voltage at its surface and prevent the deposition of a conductive layer over the insulating ceramic.

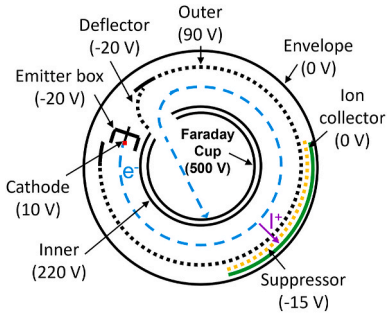

Fig. 1. Gauge configuration and voltages predicted by simulation.

The ceramic balls provide sufficient electrical insulation between the electrodes for the safe and proper gauge operation. Since, ion current in the order of picoamps or lower is expected in the UHV range the ion collector requires and electrical insulation greater than 100 TΩ. Failure to maintain this insulation would lead to leakage currents to the ion collector, significantly affecting the measured ion current. To ensure proper insulation, two protective ring-shaped electrodes connected to ground were installed, one on each side of the ion collector base. This provides that any eventual leakage current from adjacent electrodes will pass to these shielding electrodes, not to the ion collector.

The suppressing grid had to be fixed differently from the other electrodes due to its significantly reduced thickness (0.2 mm). It was attached to the outer electrode using ceramic bushings to ensure electrical insulation.

2.2. Conductance of the top plate

Assembling the gauge within the chamber, as illustrated in Fig. 2, is not advisable due to the potential penetration of external fields and the risk of electrons or ions escaping. Therefore, it is essential to incorporate a grounded top plate for electrical shielding. However, it is crucial to verify that this cover possesses sufficient conductance to prevent any notable pressure difference between the interior of the gauge and the connected chamber.

Ionisation gauges also operate as a vacuum pump. The ionic current sputters the collector producing coatings resulting in gas 'condensation' inside the gauge. Another mechanism is the chemical pumping, once gas particles impinge the filament, they can dissociate and generate radicals that will be pumped by the surrounding electrodes surfaces [19]. On the other hand, outgassing from electrodes and filament contributes to an increase in pressure inside the gauge. While pumping due to ionisation can be easily estimated, outgassing is strongly dependent on surface cleanliness and history. However, the latter can be effectively decreased by proper baking in vacuum.

The top plate was designed with 10 circular openings, each measuring 10 mm in diameter. Since the area of the openings is about 150 times greater than the area of the filament, even if all the particles impinging the filament dissociate, the chemical pumping will not significantly influence the measurement accuracy.

According to common approximations for apertures in the molecular flow regime [20], the estimated conductance for N2 at room temperature is 93 L/s. However, precise geometry simulations conducted using MolFlow + software [21] resulted in a conductance value of 60 L/s. The pumping speed due to ionisation was calculated based in the total ion current produced, including that not collected, as 1.4×10^{-3} L/s. Consequently, the top plate apertures demonstrate sufficient conductance to ensure pressure homogeneity inside and outside the gauge.

2.3. Electrical connections and controller

A dedicated controller was assembled to power the gauge, providing all the necessary voltages to bias the electrodes and the current for heating the filament. It features six regulated voltage sources and a floating current. The emission current can be adjusted and kept constant in the range 0–100 μA. The ion current is extracted through a BNC connector and measured by a picoammeter (RBD Instruments, model 9103 USB Picoammeter), which delivers a digital signal. This signal is

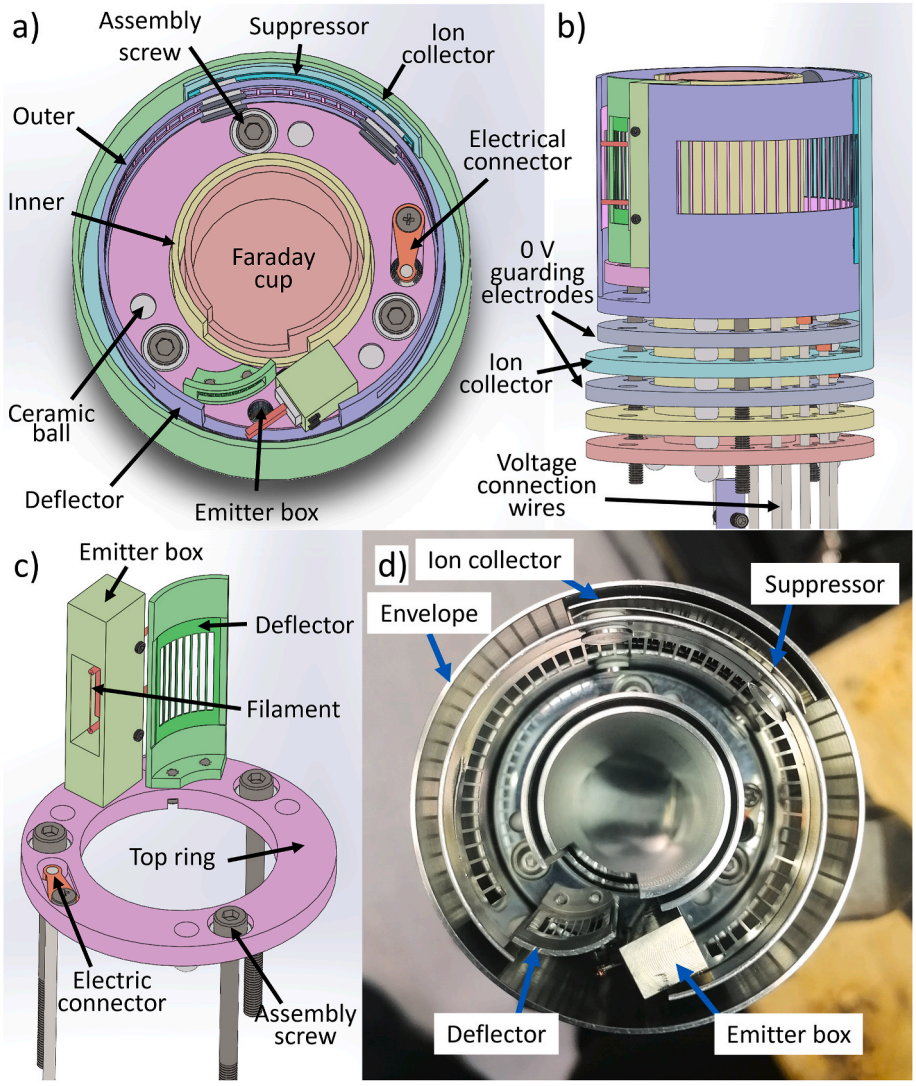

Fig. 2. Cylindrical gauge: a) CAD top view of the gauge, without the top plate of the envelope; b) CAD side view, without the envelope and the top plate; c) CAD assembly of the top ring with the emitter box and the deflector; d) photography from the top; e) electrical connections to the flange.

then read and processed by a Python software application running in an ordinary computer.

All electrical connections in the vacuum side are made by Kapton coated wire (silver-plated copper conductor). These wires have shown to introduce a limitation in the low pressure end due to outgassing as discussed ahead.

3. Operational tests and metrological evaluation

The gauge was assembled inside a tube connected via a CF-40 port to a vacuum chamber, pumped by a 300 L/s turbomolecular pump and a rotary vane pump. A MKS SRG-2 spinning rotor gauge, calibrated for N_2, was used as reference standard and traceability - calibration certificate nº9497 DKD, 2020-07, THM laboratory, Germany. The pressure of other gases was measured also by the SRG by introducing the molar mass of that gas in the controller. The set-up used for these tests is commonly employed by the laboratory to perform accredited calibrations of vacuum measurement devices.

Before any test, the system was baked at temperatures between 130 and 150 °C for at least 36 h. Subsequently, the gauge was left connected overnight. After reaching the base pressure of the system, low 10^{-8} mbar, the offset of the SRG was adjusted so that the base pressure of the system corresponded to zero. The same procedure was applied to the cylindrical gauge, subtracting the background ion current corresponding to the base pressure of the system from each measurement. Thus, the pressure measured by the gauges corresponded only to the gas pressure introduced into the calibration system, assuming that the base pressure does not change significantly during the calibration period.

3.1. Electron transmission and suppression of ion induced secondary electrons

The optimal potentials for each electrode, as depicted in Fig. 1, were initially determined through simulations and are published in the previous work [17]. Once the prototype was assembled, the electrode potentials were varied to find the actual potentials that maximize the gauge's performance. The most critical voltages are those responsible for the proper collection of electrons in the Faraday cup and for the suppression of secondary electrons from the ion collector. For this evaluation the pressure was approximately 1×10^{-5} mbar of N_2.

In general, the optimal potentials closely aligned with the predictions from the simulations, requiring no adjustments for the gauge to function properly. The electron transmission achieved was 99.8 %, defined as the ratio of the electron current collected in the Faraday cup to the emitted current from the cathode [16]. Testing up to a maximum emission current of 100 μA revealed no discernible influence of space

charge effects on the gauge's operation.

The transmission is mainly determined by the Faraday cup and the emitter box voltages, once other voltages are well tuned. Higher voltage in the Faraday cup increases the potential well avoiding the escape of low energy secondary electrons and reduce the probability of elastically scattered electrons (that can always escape the Faraday cup) [22]. The cup voltage was varied from 230 V (the same voltage of the inner electrode) up to 500 V, as shown in Fig. 3a). The transmission increased, reaching 99.8 % for a voltage above 460 V, as foreseen by simulation.

The potential of the emitter box, responsible for narrowing the beam, was also varied from 0 to −40 V. It was found that below −36 V the maximum transmission was achieved (Fig. 3b). For potentials higher than this, it is not sufficiently repulsive, widening the beam and producing collisions with the inner electrode.

The voltage of the suppressor grid has a critical effect on the measured ion current. It was varied in the range 0 to −20 V, as shown in Fig. 3c). There is a sharp drop of the ion current after −5 V, followed by signal stabilization. This result confirms the effective suppression of secondary electron emission, apparently increasing the measured ion current. Besides it appears that the secondary electron yield in this case was about 4.7 %, being of the expected order of magnitude [23]. By suppressing this undesired phenomenon, the stability of the gauge sensitivity is no longer dependent on the surface conditions of the ion collector, which is a significant advantage over most of the existing designs of ionisation gauges.

The voltage applied to the emitter box was the only potential that differed from the simulation results (−20 V). This difference is likely due to the difficulty of realistically simulating thermionic emission in the filament surface and the low particle velocity in this zone, where phenomena not considered in the simulations become more significant, such as space charge or stray magnetic fields. Nevertheless, experimental tests demonstrated that increasing the repulsion of the emitter box is sufficient to keep the beam narrow as desired.

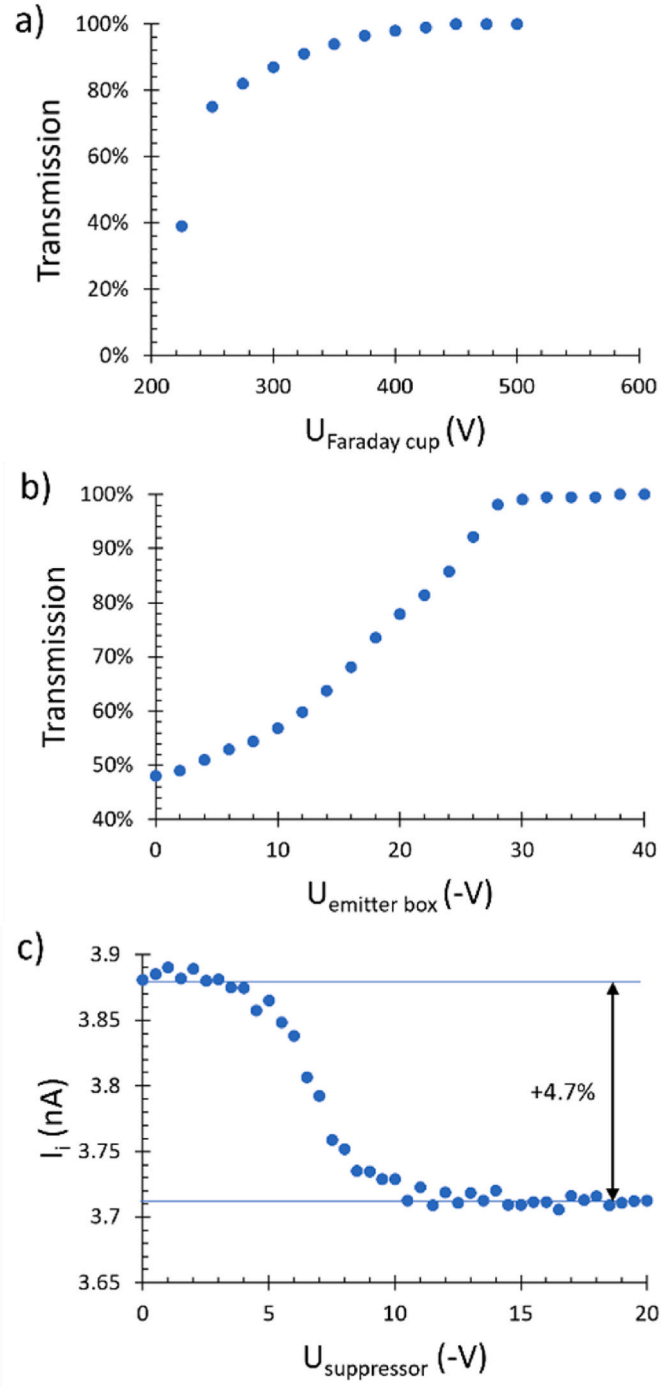

Fig. 3. Effect of critical electrode voltages on the gauge performance: a) and b) effect of Faraday cup and emitter box voltages on the electron transmission; c) collected ion current as a function of suppressor electrode voltage.

3.2. Sensitivity for different gases

To determine the sensitivity for different gases, the increase of the ion current was measured for different gas flows, while the pressure change was measured using the SRG. The gauge's sensitivity, S_{exp}, was then calculated based on the equation

$$S_{exp} = \frac{I_c - I_{c0}}{I_e \bullet (p - p_0)} \quad (4)$$

where I_c represents the collected ion current, I_e the emitted electron current, and p the pressure measured by the reference gauge while I_{c0} and p_0 represent the ion current and the residual gas pressure, respectively. The obtained sensitivity curves are represented in Fig. 4. The mean sensitivity along with their standard deviations over each curve are presented in Table 1.

Evaluation tests were not performed at pressures below 1×10^{-7} mbar, due to the limit imposed by the dispersion of the SRG measurements and to the base pressure of the system, which was only one order of magnitude lower. It was observed that points causing the highest deviation from the mean were those corresponding to lower pressures, as the sensitivity did not show a clear upward or downward trend.

The sensitivity values predicted by simulation were systematically lower than those obtained experimentally. The most plausible cause for

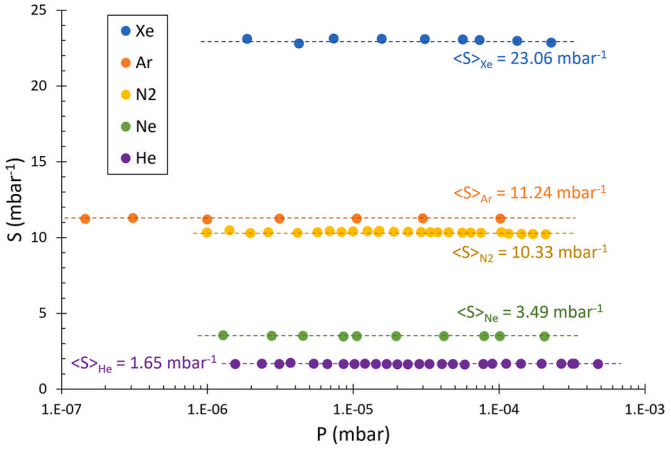

Fig. 4. Experimental sensitivity curves for different gases.

Table 1
Average sensitivity for different gases and comparison with simulation.

Gas	He	Ne	N_2	Ar	Xe
S_{exp} ($mbar^{-1}$)	1.65	3.49	10.33	11.24	23.06
σ (%)	0.98	0.59	0.61	0.26	0.77
S_{sim} ($mbar^{-1}$)	1.5	3.0	10.0	10.1	20.7
Deviation from simulation	−9.1 %	−14.0 %	−3.2 %	−10.1 %	−10.2 %

this systematic error is associated with the transparency of the grids in simulation. The grid pillars in the simulations are slightly wider than they are in the prototype, due to the resolution limitation introduced of the simulation method (finite differences). This leads to an artificial reduction in the grid transparency, decreasing the number of collected ions and, consequently, the sensitivity. This difference results in a constant offset to higher values of the sensitivity for all gases. The dispersion of the relative deviation is certainly linked to other sources inherent to the simulation or discrepancies between the actual ionisation cross-section and that used in the simulation for each gas.

3.3. Repeatability, reproducibility and linearity error

To characterise the short-term metrological performance of the gauge the repeatability, reproducibility, and linearity error was evaluated, with a coverage factor k = 1. These tests were performed with Argon in the same set-up. Repeatability was calculated by the standard deviation of S_{exp} in 10 consecutive measurements at the pressure 1.0×10^{-5} to 1.1×10^{-5} mbar. The chamber pressure was brought to this value and then pumped down to the base pressure ten times consecutively. The relative standard deviation of the sensitivity values was 0.086 %, corresponding to variations of 8.6×10^{-9} mbar. However, taking 10 consecutive measurements of the system base pressure with the SRG, a standard deviation of 4×10^{-9} mbar was obtained. The measured repeatability encompasses the pressure measurement dispersion, and thus the measurement represent an upper limit to uncertainty associated with repeatability.

Reproducibility is calculated as the standard deviation of sensitivity from 3 different measurements conducted in consecutive days. To achieve this, the sensitivity was assessed at several pre-defined pressure values. The linearity error was calculated as the difference between the sensitivity for each pressure and the mean sensitivity for the entire tested pressure range. Fig. 5 shows the relative values of the reproducibility and the linearity error. These two parameters remained below 1 % throughout the entire pressure range, indicating that sensitivity can be considered constant within a range not exceeding 1 % in the short term.

The values obtained for these three parameters are of the same order of magnitude as other well-known gauges such as ISO, extractor or Stabil-ion gauges [11,15,24,25]. The results presented demonstrate high short-term stability, but do not provide conclusions about long-term stability, where sensitivity can undergo much higher changes.

3.4. Evaluation under UHV

Additional studies were performed at CERN in dedicated an ultra-high vacuum (UHV) system. The aim was to verify if the sensitivity of the gauge remained constant at pressures lower than 10^{-7} mbar. The gauge was exposed to air during the transportation, which took about one week. It was installed in a chamber pumped by a turbo-molecular pump, with rotary pump, able to reach the pressures in the low 10^{-10} mbar range after proper baking. Pressure measurements were taken using a commercial BARION ionisation gauge from VACOM, an MKS SRG-3, a compact capacitive gauge from PFEIFFER, and one of the newly developed 'ISO' gauge [14–16,26]. Before initiating calibrations, a 24 h baking process was conducted at a temperature of 150 °C throughout the chamber including the gauge heads. During the cooling process, all hot cathode ionisation gauges were turned on to prevent adsorption of gases released during the filament outgassing onto adjacent electrodes. The gauges remained active overnight, and the first calibration was performed the following day. The system's base pressure before the calibration was 1.1×10^{-8} mbar.

Ion currents from both gauges, the cylindrical gauge and the 'ISO' gauge, were measured and compared with the BARION gauge, which had been used before to measure pressures down to approximately 10^{-11} mbar. Sensitivity for N_2 was determined using Equation (4), using the BARION reading as reference. Calibrations were conducted from the lowest to the highest pressure, by introducing nitrogen through a manual sapphire-sealed leak valve. No surface conditioning of the ion collectors of any gauge was performed before obtaining the first sensitivity curve, contrary to the recommended procedure for achieving high stability of the ISO gauge [14]. The sensitivity of the ISO gauge was found to vary considerably, with a relative standard deviation of 4.8 % (Fig. 6). The cylindrical gauge maintained a more stable sensitivity across the entire pressure range, exhibiting a relative standard deviation of 2.9 %.

Gauges were then conditioned by exposing them to a pressure of 1×10^{-4} mbar for 15 min to enhance ion bombardment on the collector surface and stabilize the secondary emission. The system was then pumped down to the pressure of 6.4×10^{-9} mbar without additional baking. A new calibration was performed, in the range 1.8×10^{-9} to 3.3×10^{-4} mbar of N_2. As depicted in Fig. 7, the sensitivity of the cylindrical gauge remained unchanged, while the ISO gauge improved its stability in the entire pressure range. This result confirms the high

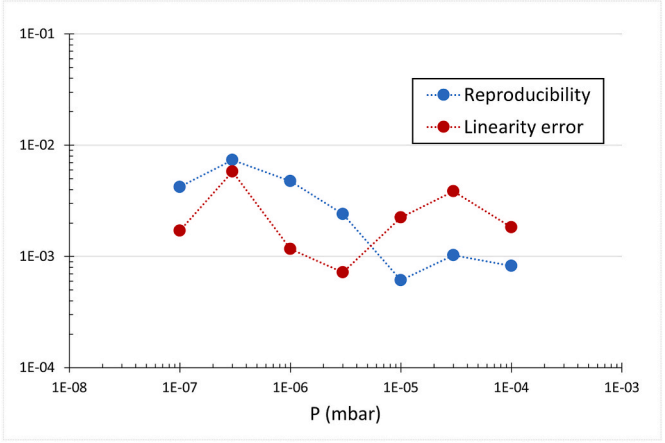

Fig. 5. Relative reproducibility and linearity errors measured with argon gas.

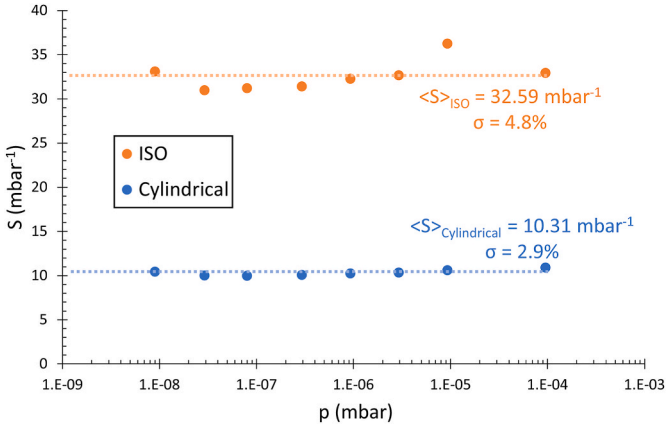

Fig. 6. Sensitivity curves of the cylindrical and ISO gauges before the high pressure conditioning.

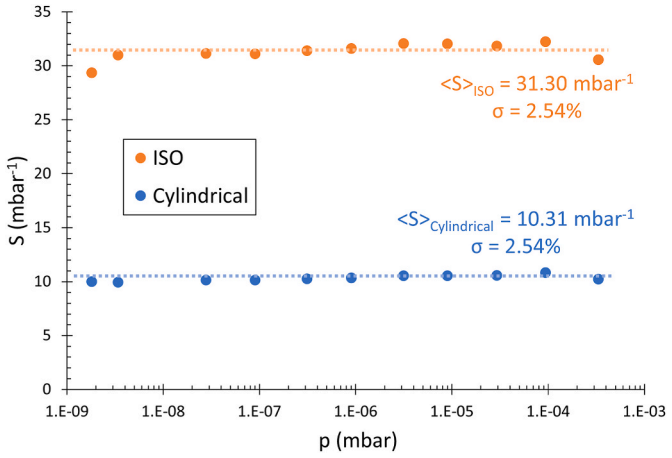

Fig. 7. Sensitivity curves of the cylindrical and ISO gauges after high pressure conditioning.

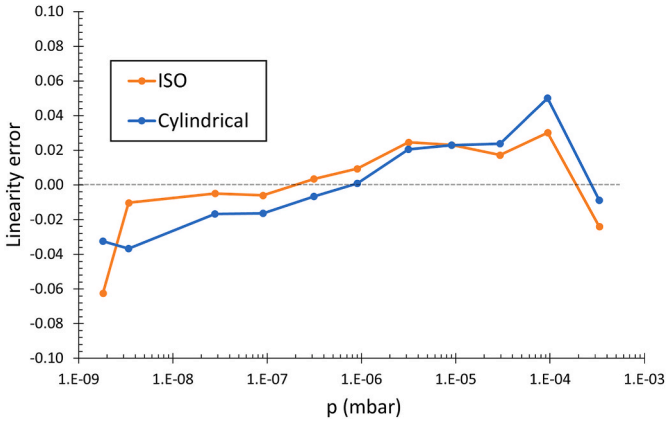

Fig. 8. Linearity error of the cylindrical and ISO gauges.

stability of the cylindrical gauge, which is independent of the ion collector surface conditions. Therefore, the cylindrical gauge does not appear to require exposure to high pressure for secondary emission to stabilize, unlike the ISO gauge that achieves its excellent stability only after the conditioning. In other words, the suppression of secondary electrons emitted from the ion collector of the cylindrical gauge is a step forward to improve the measurement stability.

In this last calibration, both gauges exhibited about the same relative standard deviation of sensitivity, 2.54 %. To investigate the cause of this similar standard deviation the linearity error was calculated for both gauges, as presented in Fig. 8. As observed, curves closely follow each other throughout the entire calibration range. This high correlation strongly suggests that the real cause for the apparent deviations displayed by both gauges is the non-linearity of the BARION gauge. The identical standard deviations of the cylindrical and ISO gauges and the correlation between their measurements is highlighting the limited accuracy of the BARION gauge.

The cylindrical gauge has shown an important limitation regarding its low-pressure limit due to outgassing. The likely reason for this pressure limitation is the desorption of water from the Kapton coatings on the connecting wires. The total area of Kapton covering all wires used in the gauge is estimated to be 28 cm^2, with a thickness of 0.15 mm. Several studies have investigated the time and temperature required to outgas polymers used in vacuum insulation [27], revealing that it is strongly linked to its thickness. Battes et al. [28] demonstrated that 100 h of baking at 100 °C is insufficient for the effective reduction of water desorption in Kapton foils with thicknesses between 0.05 and 0.127 mm. As the Kapton thickness used in the cylindrical gauge exceeds 0.127 mm the 24 h baking process was certainly insufficient. However, this limitation can be easily overcome using nude rigid wires, which is planned for a newer version of the cylindrical gauge.

4. Overview and conclusions

The presented work focused on the construction and metrological evaluation of a novel ionisation gauge which was designed for improving the measurement accuracy. The primary aim was to bridge the simulation predictions with the practical implementation, evaluating the gauge's performance within the HV and UHV ranges.

Minimal adjustments were necessary to secure optimal operation regarding the electrode voltages predicted by simulations. This not only stresses the reliability of simulations but also highlights the robustness of both the design and technical implementation. This features certainly contribute to improve the reliability and consistency in pressure measurements that can be crucial for various scientific and industrial applications. A small underestimation in the sensitivity was observed, likely due to limitations in geometric resolution during simulations.

Metrological evaluation of this gauge demonstrated high short-term stability, with repeatability, reproducibility, and linearity error consistently below 1 %, placing the gauge among the most stable ionisation gauges available over 6 orders of magnitude [11,15,24,25]. Its accuracy to measure pressures bellow 10^{-9} mbar is still open, warranting further investigation.

A significant feature is its accuracy independence of conditioning. By incorporating a suppressor grid in front of the ion collector, the gauge reading remains unaffected by changes of ion-induced secondary electron yield. This feature streamlines operational processes, ensuring enhanced stability in both short and long-term usage.

In conclusion, the cylindrical gauge appears to be a practical and stable instrument for high and ultra-high vacuum measurements, offering high accurate pressure measurements even under varying electrode surface conditions. This suggests its suitability for a wide range of fields whenever high accuracy is required.

CRediT authorship contribution statement

Ricardo A.S. Silva: Writing – original draft, Visualization, Validation, Software, Methodology, Investigation, Formal analysis, Data curation, Conceptualization. **Nenad Bundaleski:** Writing – review & editing, Supervision, Methodology, Funding acquisition, Conceptualization. **Berthold Jenninger:** Resources, Methodology. **Orlando M.N.D. Teodoro:** Writing – review & editing, Validation, Supervision, Resources, Project administration, Methodology, Funding acquisition, Conceptualization.

Declaration of competing interest

The authors declare the following financial interests/personal relationships which may be considered as potential competing interests.

Data availability

Data will be made available on request.

Acknowledgements

The support of the Portuguese Foundation for Science and Technology via the grants UIDB/00068/2020 and UIDP/00068/2020 is gratefully acknowledged. One of the authors (R.A.S. Silva) would like also to express his gratitude to the Portuguese Foundation for Science and Technology for his scholarship UI/BD/150626/2020.

References

[1] K. Jousten, Handbook of Vacuum Technology, Wiley-VCH, Weinheim, Germany, 2016, pp. 565–639.

[2] K. Jousten, F. Boineau, N. Bundaleski, C. Illgen, J. Setina, O.M.N.D. Teodoro, M. Vicar, M. Wüest, A review on hot cathode ionisation gauges with focus on a suitable design for measurement accuracy and stability, Vacuum 179 (2020), https://doi.org/10.1016/j.vacuum.2020.109545.

[3] O.E. Buckley, An Ionization Manometer, vol. 2, Proceedings of the National Academy of Sciences, 1916, pp. 683–685.

[4] G. Haas, H.-S. Bosch, In Vessel Pressure Measurement in Nuclear Fusion Experiments with ASDEX Gauges, 1998.

[5] R.T. Bayard, D. Alpert, Extension of the low pressure range of the ionization gauge, Rev. Sci. Instrum. 21 (1950) 571–572, https://doi.org/10.1063/1.1745653.

[6] P.A. Redhead, New hot-filament ionization gauge with low residual current, J. Vac. Sci. Technol. 3 (1966) 173–180, https://doi.org/10.1116/1.1492470.

[7] J.C. Helmer, W.H. Hayward, Ion gauge for vacuum pressure measurements below 1×10−10 torr, Rev. Sci. Instrum. 37 (1966) 1652–1654.

[8] F. Watanabe, Ion spectroscopy gauge: total pressure measurements down to 10 −12 Pa with discrimination against electron-stimulated-desorption ions, J. Vac. Sci. Technol. A: Vacuum Surf. Films 10 (1992) 3333–3339, https://doi.org/10.1116/1.577821.

[9] F. Watanabe, Bent belt-beam gauge: extending low-pressure measurement limits in a hot-cathode ionization vacuum gauge by combining multiple methods, J. Vac. Sci. Technol. A: Vacuum Surf. Films 28 (2010) 486–494, https://doi.org/10.1116/1.3400233.

[10] N. Takahashi, J. Yuyama, Y. Tuzi, H. Akimichi, I. Arakawa, Axial-symmetric transmission gauge: extension of its pressure measuring range and reduction of the electron stimulated desorption ion effect in ultrahigh vacuum, J. Vac. Sci. Technol. A: Vacuum Surf. Films 23 (2005) 554–558, https://doi.org/10.1116/1.1901668.

[11] P.C. Arnold, D.G. Bills, M.D. Borenstein, S.C. Borichevsky, Stable and reproducible Bayard-Alpert ionisation gauge, J. Vac. Sci. Technol. 12 (1994) 580–586.

[12] L.G. Pittaway, Electron trajectories in ionization gauges, J. Phys. D Appl. Phys. 3 (1970) 1113. http://iopscience.iop.org/0022-3727/3/7/316.

[13] A. Klopfer, An ionization gauge for measurement of ultra-high vacuum, in: Trans. 8th Nat. Vacuum Symp, 1961, pp. 439–442.

[14] K. Jousten, M. Bernien, F. Boineau, N. Bundaleski, C. Illgen, B. Jenninger, G. Jönsson, J. Šetina, O.M.N.D. Teodoro, M. Vičar, Electrons on a straight path: a novel ionisation vacuum gauge suitable as reference standard, Vacuum 189 (2021), https://doi.org/10.1016/j.vacuum.2021.110239.

[15] K. Jousten, S. Bechstein, M. Bernien, F. Boineau, N. Bundaleski, C. Illgen, B. Jenninger, J. Šetina, R.A.S. Silva, A. Stöltzel, O.M.N.D. Teodoro, M. Wüest, Evaluation and metrological performance of a novel ionisation vacuum gauge suitable as reference standard, Measurement 210 (2023), https://doi.org/10.1016/j.measurement.2023.112552.

[16] B. Jenninger, J. Anderson, M. Bernien, N. Bundaleski, H. Dimitrova, M. Granovskij, C. Illgen, J. Setina, K. Jousten, P. Kucharski, C. Reinhardt, F. Scuderi, R.A.S. Silva, A. Stöltzel, O.M.N.D. Teodoro, B. Trzpil-Jurgielewicz, M. Wüest, Development of a design for an ionisation vacuum gauge suitable as a reference standard, Vacuum 183 (2021), https://doi.org/10.1016/j.vacuum.2020.109884.

[17] R.A.S. Silva, N. Bundaleski, O.M.D.N. Teodoro, Cylindrical hot cathode ionisation gauge – the concept and simulations, Vacuum 219 (2024), https://doi.org/10.1016/j.vacuum.2023.112701.

[18] D.G. Bills, Causes of nonstability and nonreproducibility in widely used Bayard–Alpert ionization gauges, J. Vac. Sci. Technol. A: Vacuum Surf. Films 12 (1994) 574–579, https://doi.org/10.1116/1.578836.

[19] A. Stöltzel, B. Jenninger, Comparison of ionization vacuum gauges close to their low pressure limit, Vacuum 207 (2023), https://doi.org/10.1016/j.vacuum.2022.111573.

[20] M.H. Hablanian, High-Vacuum Technology: A Practical Guide, second ed., Routledge, New York, 2017 https://doi.org/10.1201/9780203751923 (Chapter 3).

[21] CERN, MolFlow+ website. https://molflow.web.cern.ch/, 2023. (Accessed 23 November 2023).

[22] N. Bundaleski, C.F. Adame, M. Bernien, C. Illgen, B. Jenninger, K. Jousten, F. Scuderi, R.A.S. Silva, A. Stöltzel, J. Šetina, O.M.N.D. Teodoro, T. Verbovšek, M. Vičar, M. Wüest, Novel ionisation vacuum gauge suitable as a reference standard: influence of primary electron trajectories on the operation, Vacuum 201 (2022), https://doi.org/10.1016/j.vacuum.2022.111041.

[23] I. Figueiredo, N. Bundaleski, O.M.N.D. Teodoro, K. Jousten, C. Illgen, Influence of ion induced secondary electron emission on the stability of ionisation vacuum gauges, Vacuum 184 (2021), https://doi.org/10.1016/j.vacuum.2020.109907.

[24] H. Yoshida, K. Arai, H. Akimichi, M. Hirata, Stability tests of ionization gauges using two-stage flow-dividing system, Vacuum 84 (2009) 705–708, https://doi.org/10.1016/j.vacuum.2009.09.011.

[25] D. Li, K. Jousten, Comparison of the stability of hot and cold cathode ionization gauges, J. Vac. Sci. Technol. A: Vacuum Surf. Films 21 (2003) 937–946, https://doi.org/10.1116/1.1578654.

[26] M. Bernien, M. Götz, C. Illgen, D. Drung, C. Krause, T. Bock, K. Jousten, Traceable low-current measurements for a novel ionization gauge suitable as reference standard, in: Measurement: Sensors, Elsevier Ltd, 2021, https://doi.org/10.1016/j.measen.2021.100202.

[27] S.G. Sammartano, I. Wevers, G. Bregliozzi, P. Chiggiato, in: Te-Vsc, Outgassing Rates of PEEK, Kapton ® and Vespel ® Foils, 2021. Geneva, https://cds.cern.ch/record/2723497. (Accessed 6 November 2023).

[28] K. Battes, C. Day, V. Hauer, Outgassing behavior of different high-temperature resistant polymers, J. Vac. Sci. Technol. A: Vacuum Surf. Films 36 (2018), https://doi.org/10.1116/1.5001243.